ResearchGate

See discussions, stats, and author profiles for this publication at: https://www.researchgate.net/publication/353274513

Towards engineering heart tissues from bioprinted cardiac spheroids

Article *in* Biofabrication · July 2021

DOI: 10.1088/1758-5090/ac14ca

CITATIONS
2

READS
95

19 authors, including:

Liudmila Polonchuk
Roche
71 PUBLICATIONS **1,392** CITATIONS
SEE PROFILE

Lydia Surija
The University of Sydney
3 PUBLICATIONS **3** CITATIONS
SEE PROFILE

Poonam Sharma
The University of Newcastle, Australia
17 PUBLICATIONS **34** CITATIONS
SEE PROFILE

Clara Liu Chung Ming
University of Technology Sydney
9 PUBLICATIONS **7** CITATIONS
SEE PROFILE

Some of the authors of this publication are also working on these related projects:

Project 3D in vitro model of Myocardial I/R Injury View project

Project Multifunctional Nanoparticles from Plasma Dust for Biomedical Applications View project

All content following this page was uploaded by Carmine Gentile on 18 July 2021.

The user has requested enhancement of the downloaded file.

Towards Engineering Heart Tissues from Bioprinted Cardiac Spheroids

Liudmila Polonchuk[1], Lydia Surija[2], Min Ho Lee[2], Poonam Sharma[2,3,4], Clara Liu Chung Ming[4], Florian Richter[2], Eitan Ben-Sefer[4], Maryam Alsadat Rad[4], Hadi Mahmodi Sheikh Sarmast[4], Wafa Al Shamery[4], Hien Tran[5], Laura Vettori[4], Fabian Haeusermann[1], Elysse C. Filipe[6,7], Jelena Rnjak-Kovacina[5], Thomas Cox[6,7], Joanne Tipper[4], Irina Kabakova[4], Carmine Gentile[2,4,*]

[1] F Hoffmann-La Roche AG Research and Development Division, Pharmaceutical Sciences, Roche Innovation Center Basel Grenzacherstrasse 124, Basel, Basel-Stadt, CH 4070
[2] The University of Sydney Faculty of Medicine and Health, Kolling Building, Kolling Institute, St Leonards, Sydney, NSW, AUS 2065
[3] The University of Newcastle Faculty of Health and Medicine, University Dr, Callaghan AUS NSW 2308
[4] University of Technology Sydney Faculty of Engineering, Building 11, Level 10, Room 115, Ultimo, Sydney, NSW, AUS 2007
[5] School of Biomedical Engineering, UNSW Sydney, Sydney NSW, AUS 2052
[6] Garvan Institute of Medical Research, 384 Victoria St Darlinghurst, NSW, AUS 2010
[7] St Vincent Clinical School, Faculty of Medicine, UNSW Sydney, Sydney NSW, AUS 2052
* Author to whom any correspondence should be addressed.
E-mail: carmine.gentile@uts.edu.au

Supplementary material for this article is available online

Received xxxxxx
Accepted for publication xxxxxx
Published xxxxxx

Abstract

Current *in vivo* and *in vitro* models fail to accurately recapitulate the human heart microenvironment for biomedical applications. This study explores the use of cardiac spheroids (CSs) to biofabricate advanced *in vitro* models of the human heart. CSs were created from human cardiac myocytes, fibroblasts and endothelial cells, mixed within optimal alginate/gelatin hydrogels and then bioprinted on a microelectrode plate for drug testing. Bioprinted CSs maintained their structure and viability for at least 30 days after printing. Vascular endothelial growth factor (VEGF) promoted endothelial cell branching from CSs within hydrogels. Alginate/gelatin-based hydrogels enabled spheroids fusion, which was further facilitated by addition of VEGF. Bioprinted CSs contracted spontaneously and under stimulation, allowing to record contractile and electrical signals on the microelectrode plates for industrial applications. Taken together, our findings indicate that bioprinted CSs can be used to biofabricate human heart tissues for long term *in vitro* testing. This has the potential to be used to study biochemical, physiological and pharmacological features of human heart tissue.

Keywords: bioprinting, bioinks, vascularization, VEGF, fusion, spheroids, cardiac physiology

1. Introduction

Cardiovascular disease (CVD) is the leading cause of morbidity and death in the modern world.[1-4] More physiological models to study the human heart microenvironment may advance how to detect, prevent and treat CVD in the future.[5] In this context, *in vitro* testing represents an essential part of developing treatment as well as understanding underlying mechanisms of CVD. [5, 6] These include *in vitro* cardiac models utilizing human cells to test their molecular, cellular and extracellular response when they are exposed to pathophysiological conditions, currently limited by their ability to replicate the complex cardiac tissue environment.[1, 5, 7] Advanced bioengineered cardiac *in vitro* models can assist in improving current treatments by better replicating the cardiac tissue microenvironment under physiological and pathological conditions.[5] Current *in vitro* models which utilize monolayer cell cultures are limited by cells growing as a monolayer on a flat surface contrary to the three-dimensional nature of tissue. Three-dimensional (3D)

 © xxxx IOP Publishing Ltd

cultures, on the other hand, better mimic the cell structure and microenvironment found *in vivo* and provide advanced tools to improve accuracy of *in vitro* testing.[5] These cultures also improve the viability and function of cardiac cells expanding the potential for diagnostic and therapeutic applications.[8] Among several 3D cultures of cardiac cells, cardiac cell aggregates (known as " cardiac spheroids" or CSs) are used in multiple applications, including *in vitro* testing. [5, 7, 9] More recently, spheroid cultures have been employed together with 3D bioprinting technology to create *in vitro* 3D models of tissue and organs.[10] In this approach, a bioprinter deposits the biological ink (or "bioink") layer-by-layer to create a three-dimensional structure. In this manuscript, the bioink is composed of cardiac spheroid cultures embedded within tissue-specific permissive hydrogels for optimal cardiac cell viability and function. Bioprinting technology has been explored as a method to generate and use spheroids to allow for scalable, uniform and automated biofabrication of tissues.[11, 12] The potential use of bioinks composed of spheroids and hydrogels as building blocks for tissue engineering purposes have been previously explored.[13, 14] Spheroid extrusion through a micropipette nozzle occurs after spheroid generation, either by extruding spheroids alone or by embedding them within supporting hydrogels. Spheroid fusion can occur in hanging drop cultures by reducing surface tension and by promoting cell-cell adhesion.[13] During this process, the application of vascular endothelial growth factor (VEGF) plays a major role in promoting spheroid fusion within hydrogels.[13] Similarly, fusion of spheroids presenting a vascular network within hydrogels with specific viscosity is feasible.[13]

One of the most challenging tasks for the optimal bioengineering of viable and functional cardiac tissues is the recreation of its vascularization.[1, 15] As most organs and tissues in our body are fully perfused with blood, a fully vascularized 3D *in vitro* model will more accurately replicate the biochemical, morphological and physiological behavior of cells compared to existing *in vitro* models.[16-18] More recently, biofabrication of personalized cardiac tissues by 3D bioprinting of patient-derived stem cells has been explored for *in vivo* applications, including myocardial regeneration in heart failure patients to replace damaged heart tissues.[10, 19, 20] However, these approaches failed at fully generating functional tissues that completely recapitulate biochemical, morphological and physiological features typical of the *in vivo* heart, including a proper vascular network formation and contractile function. The objective of this study was the identification of optimal hydrogels using alginate and gelatin with viscoelastic properties that are similar to the ones of native cardiac tissue, while allowing cells to survive and function properly within the biofabricated tissue. This study presents a way forward in the field of cardiac bioengineering by developing an approach that better replicates the human heart microenvironment by bioprinting cardiac spheroids in hydrogels.[16, 21] The hypothesis is that cardiac spheroids can be used as building blocks to 3D bioprint *in vitro* models of the human heart within optimal alginate-based hydrogels. The goal of the present work was to evaluate different hydrogel combinations for bioprinting human cardiac spheroids and their utility for assessment of functional properties, with the potential use for testing *in vitro* of cardiac cell viability and function.

2. Material and Methods

2.1 Bioprinting

All bioprinting was carried out using either a custom-made extrusion based bioprinter from REGEMAT 3D, (Spain) or a CELLINK BioX (Sweden). The REGEMAT3D bioprinter was kept within a Biosafety Cabinet (BSC) and it was programmed through G-codes (**Figure S1**). The bioprinting procedure is captured in **Video 1**. The BioX bioprinter is a standalone system that allows a sterile environment without having to move the device to a BSC.

2.2 Hydrogel Formation and Crosslinking

Hydrogels were made by dissolving dry powders up to 30 minutes or until completely dissolved in Dulbecco's Modified Eagle's Medium – high glucose (Life Science, Sigma Aldrich) with 1% (v/v) Penicillin-Streptomycin (50 units/ml penicillin and 50 µg streptomycin/mL) and 1% (v/v) 200 mM L-Glutamine. Powders used were alginic acid sodium salt from brown algae (Al) and gelatin from bovine skin (Ge). The media was heated to 50°C, the gelatin and alginate powders were then slowly added and completely dissolved with stirring. The resulting hydrogels were divided into 15 mL aliquots and stored at 4°C.

Different hydrogel compositions were tested including: i) 2% (w/v) Al and 6 % (w/v) Ge, ii) 3% (w/v) Al and (w/v) 6% Ge, iii) 4% (w/v) Al and 8% (w/v) Ge. The hydrogel was crosslinked with a sterile 0.2 µm filtered calcium chloride solution made from 2% (w/v) calcium chloride dihydrate powder in Dulbecco's Phosphate Buffered Saline (DPBS) with no Calcium Chloride or Magnesium Chloride (Gibco, ThermoFisher Scientific) and 50 ml aliquots were stored at 4°C with the lid fully sealed with parafilm to prevent any potential evaporation. Once bioprinted, hydrogels first were crosslinked and then incubated at 37°C with culture media in presence or absence of spheroids.

2.3 Mechanical Testing of Hydrogels Using Unconfined Compression Test

The Young's modulus of hydrogel samples ($n = 3$) was measured through unconfined compression on a TA Instruments Dynamic Hybrid Rheometer (DHR-3, TA Instruments). An 8mm diameter punch biopsy was taken from each hydrogel and placed between the top and bottom geometries. Mechanical characterisation of the hydrogels was performed using unconfined compression analysis, with a constant compression rate of 10mm/min with data output in the form of axial force (N) and gap (mm). During the measurements, the axial force was changed from 0 N to 0.2 N. Results were analysed and a stress/strain curve for each replicate hydrogel was obtained. The Young's modulus (kPa) was obtained from the linear region of the stress/strain curve. All samples were measured at 25° C and on the same day.

2.4 Micromechanical Testing of Hydrogels Using Brillouin Microspectroscopy

Brillouin microspectroscopy was used to determine viscoelastic properties of all types of hydrogel materials. The Brillouin microspectroscopy system consisted of a continuous wave 660 nm Laser (Torus, Laser Quantum), a confocal microscope (CM1, JRS Instruments) and a scanning tandem Fabry-Perot interferometer (TFP1, JRS Instruments). The laser power on the sample was 50 mW, and the acquisition time per point was 1-10 s. The raw spectra, containing Rayleigh and Brillouin peaks, were fitted using the Damped Harmonic Oscillator model, and the position of the Stokes and anti-Stokes Brillouin peaks were determined with uncertainty below 10 MHz. Each gel composition was tested 12 times (4 sample repeats with 3 measurements per each sample) and the average and standard deviation in the Brillouin frequency shift (Ω) across the measurement set were determined. To avoid the effects of dehydration on gel viscoelasticity, the samples were kept in the incubator prior to the measurements at constant temperature and humidity. [22]

2.5 Pore Size Measurements in Bioprinted Hydrogels using Scanning Electron Microscopy (SEM)

In order to characterize the pore structure of bioprinted hydrogels, scanning electron microscopy (SEM) was employed. Briefly, hydrogels were first dried in a vacuum oven (100kPa) for 24 hours, then coated with platinum using a K575x Sputter coater (Emitech Quorum), and finally imaged using a S-3400 SEM system (Hitachi). Pore size was measured using at least eight random areas from each sample (two *per* day point) using ImageJ software (NIH, Bethesda) as previously described. [23]

2.6 Cell Culture and Spheroid Formation

Different cells were cultured and used: i) adult human cardiac fibroblasts (hCFs) which were cultured in DMEM with 1% (v/v) Penicillin-Streptomycin (50 units/mL penicillin and 50 µg streptomycin/mL), 1% (v/v) 200 mM L-Glutamine and 10% (v/v) Fetal Bovine Serum (FBS); ii) adult human coronary artery endothelial cells (HCAEC) which were cultured in MesoEndo Cell Growth Medium (Cell Applications, Inc); and iii) Cor.4U SC-derived cardiac myocytes, which were cultured in Cor.4U media according to manufacturer's instructions (Ncardia).

Spheroids were formed using a 384-hanging drop culture plate (Perfecta3D, 3D Biomatrix, Inc.) as previously described.[9, 22] Based on previous studies, human spheroids were formed by co-culturing 5,000 fibroblasts, 5,000 endothelial cells and 10,000 myocytes at a ratio of 1:1:2.[9, 22] A 20 µL cell suspension was added to each well and sterile DPBS was added to the side empty area of plate around the wells to prevent excessive media evaporation. The plate was incubated at 37°C for four to five days until cells aggregated and formed compact spheroids.

2.7 Staining and Imaging

Cell viability was determined using fluorescent stains diluted in DMEM. These were Nuc Blue (Life Technologies), calcein-AM and ethidium homodimer (Life Technologies) to stain for nuclei, living cells and dead cells, respectively. Cells were incubated with stains for 1 hour at 37°C in 5% (v/v) CO_2 in air.

Vascular network formation was evaluated by immunostaining for CD31 with primary mouse anti-human CD31 (BD Biosciences) and secondary Cy3-conjugated donkey anti-mouse (Jackson Laboratories) antibodies, based on previously established protocols.[9, 16] Bioprinted spheroids were also stained with mouse monoclonal [1C11] anti-human cardiac troponin T (Texas Red©) and mouse monoclonal [V9] to vimentin (Alexa 488) antibodies.

Live imaging was performed using an EVOS AUTO FL fluorescent microscope system (Life Technologies) for phase and fluorescent imaging. Confocal imaging was performed using a Zeiss LSM 800 and a Leica Stellaris WL confocal imaging system. Images were processed using NIH Fiji software and Adobe Photoshop 2021 (Adobe Systems, In., San Jose, CA, USA). For 3D reconstructions, images were processed by Imaris v 9.2 (Bitplane, Concord, MA, USA).

2.8 Functional Testing

Physiological testing of contractile activity of bioprinted spheroids was carried out on the Myocyte Contractility System (IonOptix) including an AE31 Trinocular microscope

(Motic), MyoCam-S3, MyoPacer Field Stimulator and Fluorescence System Interface (FSI).
Additional functional monitoring of spheroids was performed using CardioExcyte 96 (Nanion technologies GmbH, Germany) to record extracellular field potential (EFP) and impedance signals. Spheroids were directly bioprinted in the wells of the NSP-96 plate. Medium exchange was performed according to cell supplier recommendations. Impedance signals from spontaneously beating CSs were recorded with a sampling rate of 1 ms (1 kHz), and EFP data were collected at 0.1 ms (10 kHz). Data acquisition was controlled by CardioExcyte 96 Control software as described in [22].

2.9 Computational Modelling

Surface Evolver was used for modelling spheroid fusion, in conjunction with ATOM TEXT EDITOR, which was used to edit code files.

2.10 Statistical Analyses

In order to measure the effects of VEGF on spheroid fusion, simple linear regression was performed using GraphPad Prism™ (La Jolla, CA). Experimental data from Brillouin microspectroscopy and pore size measurements are expressed as mean ± SEM (n > 4). ANOVA followed by Bonferroni post hoc test was performed using GraphPad Prism™ (La Jolla, CA).

3. Results

3.1 Optimal Hydrogel Composition

An optimal hydrogel formulation was investigated by mixing alginate (Al) and gelatin (Ge) at different concentrations. These resulting hydrogels were tested for both printability and durability using a 300 μm diameter nozzle in either a customized extrusion REGEMAT3D or a commercially available BioX bioprinter (**Figure S1**). Cardiac spheroids (CSs) were mixed within Al/Ge hydrogels and then printed in rods **(Figures 1 and S1).** Hydrogels were subsequently polymerized by direct addition an ice-cold calcium chloride solution. This allowed optimal alginate crosslinking while preventing the gelatin from liquifying at higher temperatures. As they warmed up to 37°C in the incubator, 2%Al/6%Ge (w/v) hydrogels became liquid, resulting in spreading and lower accuracy of the print, as indicated by the asterisks in **Figure 1**. This type of hydrogel had low durability showing degradation as quickly as 3 days after printing **(Figure 1).** Increasing alginate and gelatin concentration in the hydrogel improved its durability and printability, with 4%Al/8%Ge (w/v) hydrogels showing optimal stability over 3 days in culture **(Figure 1).**

Micromechanical properties of hydrogels with three different compositions of alginate and gelatin were evaluated using unconfined compression test and a Brillouin microspectroscopy technique. Since Brillouin microspectroscopy is label-free, non-contact and non-destructive method, it was used to assess properties of the gels over all stages of fabrication and their stability over time. This method is based on the interaction of light waves with thermally excited acoustic phonons.[24] The Brillouin frequency shift (Ω) is directly related to the longitudinal storage modulus M∝Ω^2, which in turn, is inverse of the gel compressibility (β=1/M). Thus, Ω is indirectly related to the gel stiffness (lower compressibility corresponds to higher longitudinal modulus and higher stiffness). **Figure 2** compares the average frequency shift (Ω) across 12 measurements for all gel compositions on the day of their fabrication, with the error bars indicating the standard deviation from the average value. All gels showed significantly higher frequency shift (Ω) compared to cell culture medium controls. However, 4%Al/8%Ge (w/v) hydrogels present the highest frequency shift throughout the two first stages of fabrication, *i.e.* before and after crosslinking. Incubation with culture media resulted in

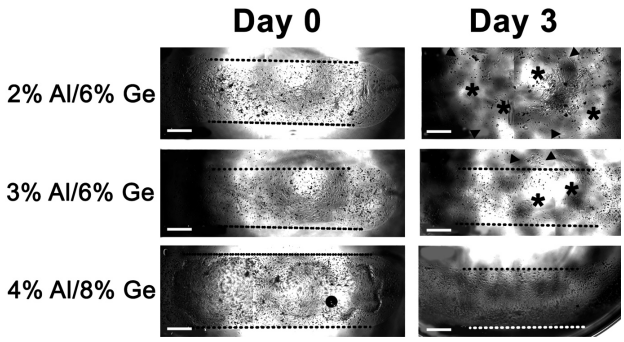

Figure 1. Durability Assessment of 3D Bioprinted Alginate/Gelatin (Al/Ge) Hydrogels in Culture Medium Over Three Days. Phase contrast microscopy images of bioprinted 2%Al/6%Ge, 3%Al/6%Ge and 4%Al/8%Ge hydrogels immediately after CaCl2 crosslinking (Days 0) and after three days (Day 3) in presence of culture medium in an incubator. Only bioprinted hydrogels containing 4%Al/8%Ge did not disintegrate after three days in culture, whereas 2%Al/6%Ge and 3%Al/6%Ge dissolved in media at the same time. Dotted lines delimit area covered by intact hydrogels after being bioprinted, asterisks point at areas where the hydrogels dissolved between the dotted lines and arrowheads point at hydrogel leaving the rod. Magnification bars equal 2 mm. For a demonstration regarding the bioprinting process, please refer to **Video 1**.

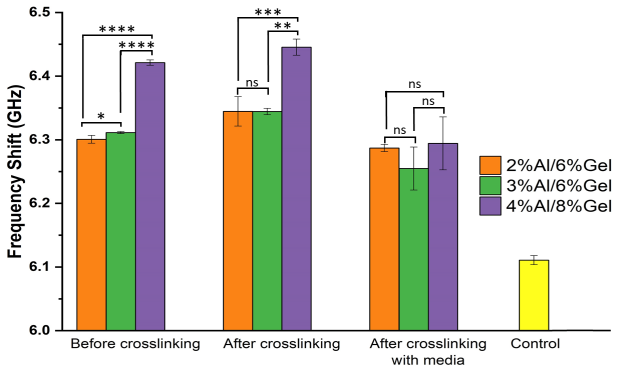

Figure 2. Brillouin Microspectroscopy Measurements of Hydrogel Viscoelasticity. Statistical analysis of hydrogels' Brillouin frequency shift measurements (GHz) [indirectly related to gel stiffness (*i.e.,* the higher the shift - the stiffer the material)]. The 4%Al/8%Gel hydrogels is the stiffest hydrogel before and after crosslinking on Day 0 of **Figure 1**. Incubation of hydrogels with culture medium resulted in softer gels and increased the variability of measurements in samples with increasing alginate concentrations. Brillouin frequency shifts for all hydrogel compositions are higher than that of the control culture medium only. (*p<0.05; **p<0.01; ***p<0.001; ****p<0.0001, n = 4).

hydrating and softening of the gels. All hydrogel formulations exhibited stiffening after the crosslinking stage and softening after incubation with medium, as expected based on poroelastic theory.[25] The latter, is most likely related to increases in gel hydration and partial gel swelling.[26] Our Brillouin microspectroscopy measurements over 14 days post fabrication of the 4%Al/8%Ge (w/v) hydrogels confirmed that presented optimal long-term stability, besides presenting the highest stiffness among the formulations tested **(Figure S2).** Our SEM analysis of bioprinted 4%Al/8%Ge (w/v) hydrogels confirmed the presence of pores for oxygen supply to cells within the construct (**Figure S3**). [23, 27, 28]

Additional measurements of hydrogels following their incubation with culture media using unconfined compression test confirmed that 4%Al/8%Ge (w/v) gel presents the highest stiffness compared to the other compositions (2%Al/6%Ge and 3%Al/6%Ge). In fact, the stiffest hydrogel has a Young's modulus of 42.23±4.34 kPa (**Figure S4**). This value falls within the range of stiffness reported for animal and human cardiac tissues.[18, 29-31]

3.2 Viability of Bioprinted Cardiac Spheroids in Al/Ge hydrogels

Cardiac cells are very sensitive to oxygen and nutrient exchange, making them more susceptible to hypoxic condition in 3D cultures.[7] Therefore, cell viability in 3D bioprinted spheroids was evaluated in 4%Al/ 8%Ge hydrogels, which were optimal for long term cultures based on this and previous studies.[10] Calcein-AM and ethidium homodimer staining showed that cells in human bioprinted spheroids maintained high viability for at least 30 days, and did not statistically change compared to similar cultures at days 7 and 14 (**Figure S5**). It is interesting to note that while some cells seemed to grow out, the overall spheroidal structure was maintained even 30 days after being bioprinted **(Figure S5).** Our evaluation of cardiac specific markers, such as cardiac troponin T and connexin 43, together with the expression of vimentin, a

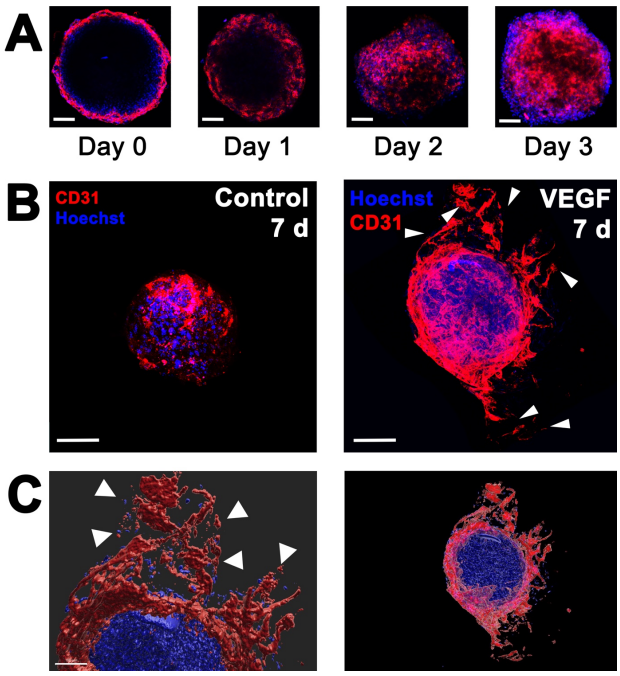

Figure 3. VEGF-mediated Angiogenesis in 3D Bioprinted Human Cardiac Spheroids within 4%Al/8%Ge Hydrogels. (**A**) Z-stacks of the center of cardiac spheroids (CSs) treated with 50ng/ml VEGF over three days in culture and imaged using a confocal microscope (CD31 in red, Hoechst stain in blue). The CD31-positive endothelial cell network extends from the outer layer to the center of the VEGF-treated CS within 3 days. (**B**) Collapsed Z-stacks taken with a confocal microscope of bioprinted CSs cultured for 7 days in the presence and absence of 50ng/ml VEGF. Arrowheads point to VEGF-induced angiogenic sprouts. CD31 (red) and Hoechst stain (blue). Magnification bars equal to 100 (**A**) and 200 (**B**) µm. (**C**) 3D rendering analysis of the VEGF-treated CS shown in (B). Arrowheads point at CD31-positive endothelial cell network that extends from the bioprinted CS into the hydrogel. For complete 3D rendering analysis of the same VEGF-treated bioprinted CS, please refer to **Video 2**.

marker of cardiac fibroblasts (**Figure S6**), confirmed the presence of the three cell types in bioprinted spheroids, in line with results from previous reports of cardiac spheroids in hanging drop culture.[16]

3.3 VEGF-mediated Vascularization of Bioprinted Spheroids

While improved vascularization remains one of the main challenges in cardiac tissue engineering, we have previously shown how vascular endothelial growth factor (VEGF), a well-known pro-angiogenic factor, is able to promote neovascularization of spheroids.[1, 7, 32] To promote new blood vessel formation, cardiac spheroids were treated with VEGF for up to 7 days. The VEGF treatment fostered vascularization as detected by CD31 immuno-staining of endothelial cells (**Figure 3**). Confocal microscopy analysis of bioprinted VCSs showed the growth of endothelial cells (ECs) from the outer cell layer towards the inner core of the CS (**Figure 3A**) and into the surrounding gel, with an increase by ~2.5 fold in CD31 staining (**Figure 3B**).

3.4 Fusion of Bioprinted Vascularized Cardiac Spheroids in Alginate/Gelatin-based Hydrogels

In order to evaluate the effects of VEGF on spheroid fusion, we measured the number of bioprinted CSs fusing over time. **Figures 4** and **S7** show how bioprinted spheroids from both control and VEGF groups undergo complete fusion over 4 days. Bioprinted spheroids appear to shrink as they fuse, with the overall size of the fused spheroids in both groups becoming smaller than the combined size of the original spheroids. This optical observation, however, does not take into account the volume of the spheroids, which was not quantitatively evaluated in this study. It is important to

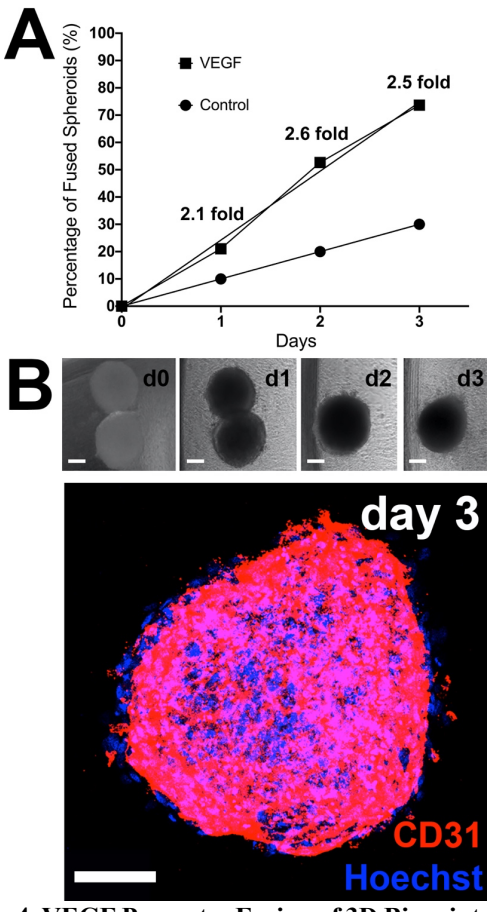

Figure 4. VEGF Promotes Fusion of 3D Bioprinted CSs within 4%Al/8%Ge Hydrogels.
(**A**) VEGF treatment of paired bioprinted CSs increased by more than 2-fold the number of completely fused spheroids after three days compared to bioprinted CSs fusing in control conditions (media only). (**B**) Phase contrast images of paired CSs fusing over three days (top panels) and collapsed Z-stacks of the fused CS (bottom panel) stained with anti-CD31 antibodies (red) and Hoechst stain (blue). Magnification bar equals 100 µm. For the 3D rendering analysis of the vascular network of the fused CS, please refer to **Video 3**.

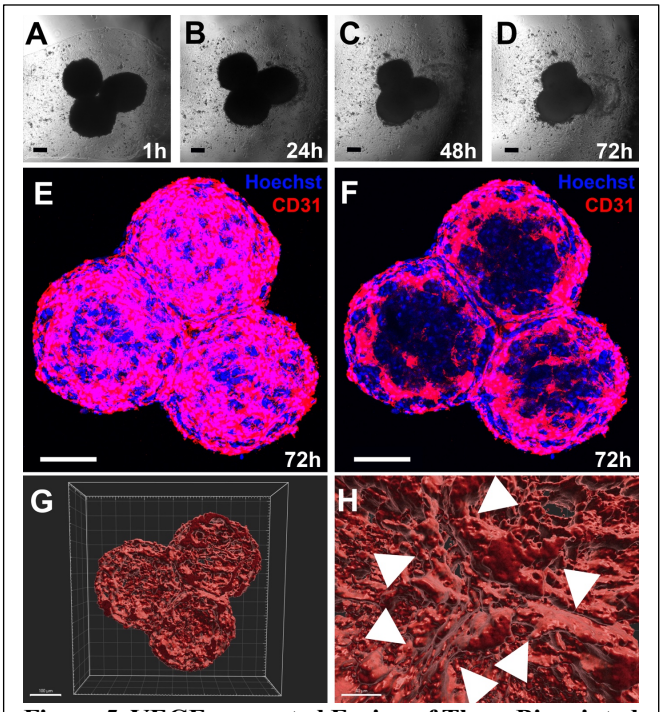

Figure 5. VEGF-promoted Fusion of Three Bioprinted Cardiac Spheroids within 4%Al/8%Ge Hydrogels. (**A-D**) Phase contrast microscopy images of three bioprinted CSs fusing within 72h. (**E**) Collapsed z-stacks of the 72h fused CSs stained with antibodies against CD31 (red) and Hoeschst stain (blue). (**F**) Confocal z-stack taken from the center of the fused CS shown in (**D**) and (**E**). (**G-H**) Low (**G**) and high (**H**) resolution of the 3D rendering analysis of the 72h fused CSs. Arrowheads point at vascular network formed at the area of contact between fused CSs. Magnification bars equal 100 µm. See also **Video 4** for animated spheroid fusion and **Video 5** for 3D rendering analysis.

highlight that spheroid fusion occurs spontaneously in bioprinted CSs (**Figure S8**).

The number of spheroids which underwent complete fusion (>75% fusion) was compared between control and VEGF-treated groups. Spheroids from both groups presented complete fusion after 1 day as shown in **Figure 4A**. The application of VEGF increased efficiency of fusion by more than 2-fold over three days compared to the control group as shown in **Figure 4B**.

Fusion of three CSs in bioprinted hydrogels generated a tissue construct where the fusion angle (120°) and directionality was maintained, as shown in **Figure 5**. Addition of VEGF to fusing CSs promoted vascular fusion detected by the CD31 staining in **Figures 5** and **S7.** The hydrogel-controlled fusion was reconstructed using computer animation as shown in **Video2**. Confocal images taken in the center of the three fused CSs showed how the CD31 endothelium is organized in between the different CSs at the end of this process **(Figure 5C).**

3.5 Functional Features of Bioprinted Cardiac Spheroid

Cardiac spheroids bioprinted in 4% Al/ 8% Ge hydrogel contracted spontaneously and upon electrical stimulation. The spheroids demonstrated spontaneous beating frequencies in the physiological range of 0.3 and 1.2 Hz, corresponding to beating rates between 18 to 72 beats per minute **(Figure 6** and **Video 6).** Contraction of CSs bioprinted in the CardioExcyte Plate induced gel movement as can be observed in **Video 7**. Bioprinted CSs also exhibited propagation of the electrical impulses, demonstrating interspheroid functional coupling as seen in **Video 8. Figure 7** shows the extracellular field potential (EFP) and impedance signals recorded from spontaneously beating cardiac spheroids bio-printed in the CardioExcyte plate. The EFP reflects their electrical activity and the impedance amplitude represents an indirect measure of contractility.[22, 33] The recording demonstrates that the spheroid constructs exhibited robust synchronous electrical activity and contractile behavior sensitive to the compound treatment. Addition of isoproterenol (1 μM) shown in **Figure 7** resulted in the increased spontaneous beating rate induced by adrenergic stimulation.

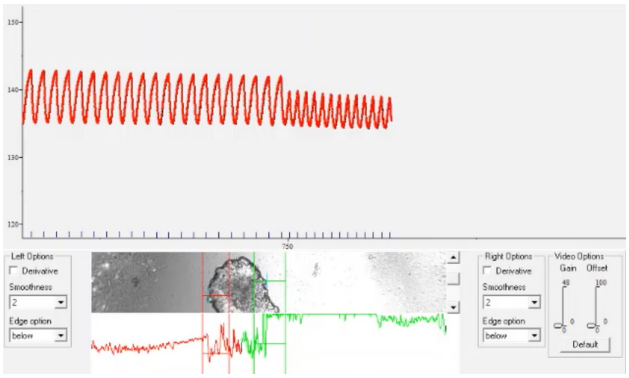

Figure 6. Field potential stimulation of a bioprinted CS. Field potential stimulation between 0.6 and 1.2 Hz was applied to record the contraction-relaxation function in bioprinted CSs using motion tracking (see also **Video 6**).

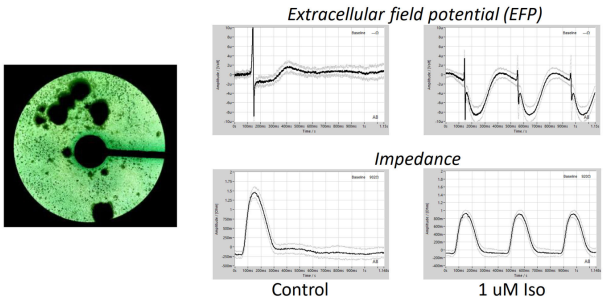

Figure 7. Electrical Recording from Bioprinted CSs using the CardioExcyte96 plate. Phase contrast image of bioprinted CSs in proximity of the electrode at the center of a well in a CardioExcyte96 plate (left). Representative measurements of raw mean beat impedance and field potential waveforms shown before and after addition of 1 μM isoproterenol to bioprinted CSs. Please refer to **Videos 7** and **8** for live recording.

4. Discussion

Modeling of physiological cardiac models remains one of the main challenges for optimal drug testing.[5, 34] Novel 3D culture systems, comprising 3D bioprinting of stem cell-derived cardiac cells has provided promising results to move this research forward.[5, 34] Nevertheless, major challenges exist with respect to achieving optimal conditions for cell viability and function.[5, 34] In this study we have shown that bioprinted cardiac spheroids comprising human cardiac endothelial cells, fibroblasts and iPSC-derived cardiomyocytes represent the optimal microenvironment for cells to grow in for long term studies (**Figures 1-2** and **S1**). This study has demonstrated how alginate/gelatin-based hydrogels with viscoelastic properties comparable to the ones of the native cardiac tissue allow optimal cell growth (**Figure S5**), tissue vascularization (**Figure 3**) and contractile function at physiological levels (**Figure 6**) and under pharmacological stimulation (**Figure 7**). Our study has demonstrated that the addition of gelatin to alginate hydrogels at 8% and 4% (respectively) generates optimal bioinks for cardiac cells to live and function properly, as previously indicated by others.[35] These soft hydrogels have a stiffness between 18.28-42.23 kPa (**Figure S4**), which recapitulate the stiffness of human myocardium (approx. 50 kPa).[18, 29-31] This stiffness is tunable depending upon the concentration of alginate, as well as the concentration of the crosslinking solution. While in our study gelatin was added to promote cell adhesion within

the hydrogel, it was not crosslinked (for instance, by addition of genipin), in order to allow cells to spontaneously populate the bioprinted hydrogels. No mass loss was detected in case of the hydrogel containing 4% (w/v) alginate and 8% (w/v) gelatin over 30 days. Our Brillouin microscopy measurements also confirmed that after crosslinking with calcium chloride, 4%Al/8%Ge bioprinted hydrogels maintain their viscoelastic properties even after addition of culture media (**Figure S2**). The printability of the hydrogel was important to achieve accurate and consistent printing (**Figure 1**). Using lower concentrations of alginate was found to reduce viscosity of the non-crosslinked hydrogel, which increased spreading and reduced accuracy of the print. At the same time, the higher concentrations of gelatin partially reduced the viscosity of the hydrogel when heated, however, this also caused the gels to solidify faster by simply lowering the temperature below 26-28 °C. It is important to note that as gelatin solidifies at room temperature, hydrogels containing higher gelatin concentrations tended to cause blockages in the print nozzles as these were not near the heating element of the bioprinter. In our study, 4%Al/8%Ge hydrogels were found to be optimal for their printability, durability and cardiac cell function. This is consistent with other studies showing that the presence of cells within a hydrogel changes its physical properties, such as viscosity.[36, 37]

Generation of a vascular tree remains one of the main challenges for the biofabrication of bioengineered heart tissues using stem cell-derived cardiac cells, influencing cell survival and function.[1, 18] While advances in 3D bioprinting of cardiac tissues have been made over the recent years, these have not provided a comprehensive and controlled vascular network for optimal cardiac function.[38-41] Bioprinting of 4%Al/8%Ge hydrogels containing CSs with high cell viability was facilitated thanks to both their pre-vascularization and the presence of pores for oxygen supply **(Figures S3** and **S5**). [23, 27, 28] Cells showed no signs of damage from the printing, crosslinking or incubation process, as which is one of the main concerns with 3D bioprinting, specifically related to shear stress.[1] Pre-vascularized spheroids retained high viability with minimal numbers of dead cells over 30 days, which supports their potential use for long term *in vitro* studies to model and evaluate complex conditions, such as ischaemia/reperfusion injury and/or cardiac fibrosis.[17]

VEGF is known for its pro-angiogenic activity *in vivo* and *in vitr*o, and it has been previously employed to promote vascular network formation in spheroids.[32, 42] VEGF is well known to promote vasculogenesis and angiogenesis via proliferation and sprouting formation from endothelial cells early during development and in adult vessels.[43] Our study shows that VEGF promoted the formation of branch-like endothelial structures within the spheroid (**Figure 3A**) and from it into the surrounding hydrogel (**Figure 3B-C** and **Video 2**). These vascular-like networks may prevent cell death in the inner core of CSs even in absence of blood flow, which would normally become apoptotic for a diameter thicker than 100-200μm.[1, 7]

The use of spheroids as building blocks and their fusion for tissue engineering has been previously explored.[13, 14] However, optimal cell viability and function in 3D bioprinted cardiac tissues using Al/Ge-hydrogels has not been previously demonstrated. Given their unique features, this presents the potential for regenerative medicine purposes to improve cardiac function following its transplantation.[19, 44] Previously, alignment of cardiac spheroids within hydrogels was established using other approaches. [45, 46] Other studies provided evidence that vascularized spheroids could be used to biofabricate complex tissues.[13, 14] This is the first study to provide a simulation of how 3D bioprinted cardiac spheroids can fused within Al/Ge hydrogels in order to be as be used as building blocks (**Video 4**). It also shows for the first time that VEGF not only promotes vascular network formation and tissue fusion in bioprinted hydrogels (**Figure 3** and **Video 2**), but it also promotes CS fusion **(Figure 4**). The fused bioprinted CS following its treatment with VEGF allows the generation of a fully vascularized tissue (**Figure 4** and **Video 3**). Hydrogel-specific properties, such as viscoelastic properties comparable to the ones found in the native cardiac tissue and the presence of bioactive gelatin for optimal cell viability, provide mechanical cues to promote tissue fusion and induce vascular network formation. This is ideal for the engineering of novel *in vitro* cardiac models, together with potential applications for regenerative medicine on a larger scale.[14] Spheroid proximity is critical for optimal fusion in hydrogels, as previously demonstrated.[45, 46] In this study we evaluated the spontaneous CS fusion process occurring in presence or absence of VEGF. In this process, VEGF was able to promote fusion of bioprinted CSs at a faster rate compared with control bioprinted cultures. Other studies have focused on the controlled fusion by using other approaches.[45, 47] Further studies should evaluate the exact relationship between the initial distance between spheroids and optimal fusion in hydrogels with different characteristics. Our simulation of spheroid modeling highlighted how partial fusion for diverse geometrical shapes can be achieved based on hydrogel-specific features (**Figure 5** and **Videos 4** and **5**).

As the use of *in vitro* bioprinted spheroids for pharmacological testing requires detectable contractile function, we evaluated how to detect it with two different methods developed by us. In our first approach, we used a Ionoptix system to measure

spontaneous contractile activity and under field potential (**Figure 6** and **Video 6**). While we were not able to measure any contractile activity in 3D bioprinted single cells, our physiological testing using cardiac cells determined that 4%Al/8%Ge hydrogels were permissive for intrinsic contractile function (**Figure 6** and **Video 6**). Bioprinted spheroids displayed spontaneous contraction towards their center. However, these movements were very small and difficult to detect. The edges of the spheroid were largely unaffected by the intrinsic contraction and it was not possible to measure any contraction. However, these cardiac spheroids responded by synchronous contraction to electrical stimulation. This may be due to the close proximity of the cells in the spheroid allowing for intracellular communication and formation of electroconductive networks.[18] The presence of connexin 43 in bioprinted CS, together with cardiac troponin T (**Figure S6**), both cardiac specific markers and essential for optimal cardiac tissue conductivity and contractility was supporting the ability of the CS to contract as a whole tissue. Spheroids could be paced between 18 and 72 beats per minute (0.3 to 1.2Hz) spanning bradycardic and normal heart rate ranges in humans. This suggests that 3D bioprinted CSs have the potential to investigate long- and short-term effects of pharmaceuticals on the human heart, a much needed response to provide novel pathophysiological tools for cardiovascular drug discovery and toxicity.[5, 34]

The EFP signal recording from spheroids showed that their electrical activity was sensitive to isoproterenol (**Figure 7**). However, the concomitant decrease in contractile signal indicated that bioprinted CSs still retain a negative force-frequency relationship known for iPSC-derived cardiomyocytes. Electrical stimulation of iPSC-CMs has been shown to improve their maturation status and function[11] A similar approach could be applied to the CSs bioprinted in the new CardioExcyte plate with built-in electrical stimulation to improve their performance and utility for drug testing.

Future studies aiming at improving the cardiac microenvironment in bioprinted CSs may focus on the recapitulation of pathophysiological conditions, such a heart attack in a Petri dish, in presence or absence of blood flow.[5] While there has been a lot of effort in engineering a more complex system, including the onset of organs-on-a-chip (including microfluidics devices), our study is the first one that directly demonstrates the spontaneous behavior of pre-vascularized cardiac tissues in presence of developmentally relevant factors, such as VEGF.

5. Conclusion

We successfully 3D bioprinted viable and functional CSs in 4%Al/8%Ge hydrogels, which present viscoelastic properties comparable to the ones of the native cardiac tissue. Overall, our study demonstrated that extrusion-based bioprinting of CSs in cardiac-tailored hydrogels represents a promising path forward in the engineering of *in vitro* models of human heart tissue. This has great potential for re-creating the human heart environment to study normal and pathological conditions in advanced cell-based models. A future direction for this research may include the use of patient-derived cardiomyocytes from iPSCs to create *in vitro* models for precision medicine.

Acknowledgements

The authors would like to acknowledge the support of the University of Sydney (Kick-Start Grant, CDIP Grant, Cardiothoracic Surgery Research Grant), UTS (Seed Funding) and Catholic Archdiocese of Sydney (Grant for Adult Stem Cell Research), Ian Potter Foundation Grant to CG and Australian Research Council (DP190101973) to IK. We would also like to thank Assoc./Prof. Louise Cole (UTS) and Dr Imala Alvis (HRI) for the kind assistance with imaging and 3D rendering analyses of confocal images.

Conflict of interest

None

References

1. Roche, C.D.*, et al.*, *Eur J Cardiothorac Surg,* **2020,** 58(3): p. 500-510.
2. Qasim, M.*, et al.*, *Int J Nanomedicine,* **2019,** 14: p. 1311-1333.
3. Ford, T.J.*, et al.*, *Heart,* **2018,** 104(4): p. 284-292.
4. Ameri, K.*, et al.*, *Circulation,* **2017,** 135(14): p. 1281-1283.
5. Sharma, P.*, et al.*, *Small,* **2021,** 17(15): p. e2003765.
6. Caddeo, S.*, et al.*, *Front Bioeng Biotechnol,* **2017,** 5: p. 40.
7. Gentile, C., *Curr Stem Cell Res Ther,* **2016,** 11(8): p. 652-665.
8. Edmondson, R.*, et al.*, *Assay Drug Dev Technol,* **2014,** 12(4): p. 207-18.
9. Sharma, P.*, et al.*, *J Vis Exp,* **2021,** (167).
10. Roche, C.D.*, et al.*, *Front Bioeng Biotechnol,* **2021,** 9: p. 636257.
11. Zhao, Y.*, et al.*, *Cell,* **2019,** 176(4): p. 913-927 e18.
12. Jakab, K.*, et al.*, *Tissue Eng Part A,* **2008,** 14(3): p. 413-21.
13. Fleming, P.A.*, et al.*, *Dev Dyn,* **2010,** 239(2): p. 398-406.
14. Visconti, R.P.*, et al.*, *Expert Opin Biol Ther,* **2010,** 10(3): p. 409-20.

15. Wang, H.*, et al.*, *Eur J Cardiothorac Surg,* **2020**.
16. Polonchuk, L.*, et al.*, *Sci Rep,* **2017,** 7(1): p. 7005.
17. Figtree, G.A.*, et al.*, *Cells Tissues Organs,* **2017,** 204(3-4): p. 191-198.
18. Mawad, D.*, et al.*, *Adv Exp Med Biol,* **2017,** 1041: p. 245-262.
19. Roche, C.D.*, et al.*, *J Vis Exp,* **2020,** (163).
20. Noguchi, R.*, et al.*, *J Heart Lung Transplant,* **2016,** 35(1): p. 137-145.
21. Campbell, M.*, et al.*, *Methods Mol Biol,* **2019,** 2002: p. 51-59.
22. Bot, C.T.*, et al.*, *J Pharmacol Toxicol Methods,* **2018,** 93: p. 46-58.
23. Baptista, M.*, et al.*, *Biomater Sci,* **2020,** 8(24): p. 7093-7105.
24. Koski, K.*, et al.*, *Appl. Phys. Lett.,* **2005,** 87: p. 061903.
25. Johnson, D., *J. Chem. Phys.,* **1982,** 77: p. 1531-562.
26. Wu, P.J.*, et al.*, *Nat Methods,* **2018,** 15(8): p. 561-562.
27. Li, X.*, et al.*, *Front Chem,* **2018,** 6: p. 499.
28. Hwang, C.M.*, et al.*, *Biofabrication,* **2010,** 2(3): p. 035003.
29. Iyer, R.K.*, et al.*, *Curr Opin Biotechnol,* **2011,** 22(5): p. 706-14.
30. Jawad, H.*, et al.*, *J Tissue Eng Regen Med,* **2007,** 1(5): p. 327-42.
31. Axpe, E.*, et al.*, *Int J Mol Sci,* **2016,** 17(12).
32. Gentile, C.*, et al.*, *Dev Dyn,* **2008,** 237(10): p. 2918-25.
33. Zhang, X.*, et al.*, *J Pharmacol Toxicol Methods,* **2016,** 81: p. 201-16.
34. Figtree, G.A.*, et al.*, *Eur Heart J,* **2021,** 42(15): p. 1464-1475.
35. GhavamiNejad, A.*, et al.*, *Small,* **2020,** 16(35): p. e2002931.
36. Blaeser, A.*, et al.*, *Adv Healthc Mater,* **2016,** 5(3): p. 326-33.
37. Jiang, L.*, et al.*, *ACS Appl Mater Interfaces,* **2017,** 9(50): p. 44124-44133.
38. Campostrini, G.*, et al.*, *Nat Protoc,* **2021,** 16(4): p. 2213-2256.
39. Noor, N.*, et al.*, *Adv Sci (Weinh),* **2019,** 6(11): p. 1900344.
40. Maiullari, F.*, et al.*, *Sci Rep,* **2018,** 8(1): p. 13532.
41. Zhang, Y.S.*, et al.*, *Biomaterials,* **2016,** 110: p. 45-59.
42. Shibuya, M., *Genes Cancer,* **2011,** 2(12): p. 1097-105.
43. Gentile, C.*, et al.*, *Dev Biol,* **2013,** 373(1): p. 163-75.
44. LaBarge, W.*, et al.*, *Micromachines (Basel),* **2019,** 10(9).
45. Ong, C.S.*, et al.*, *Sci Rep,* **2017,** 7(1): p. 4566.
46. Ong, C.S.*, et al.*, *J Vis Exp,* **2017,** (125).
47. Daly, A.C.*, et al.*, *Nat Commun,* **2021,** 12(1): p. 753.

View publication stats